HHS Public Access

Author manuscript

*Biomaterials*. Author manuscript; available in PMC 2018 October 01.

Published in final edited form as:

*Biomaterials*. 2017 October ; 142: 124–135. doi:10.1016/j.biomaterials.2017.07.022.

# Bottom-up Assembly of Salivary Gland Microtissues for Assessing Myoepithelial Cell Function

**Tugba Ozdemir**[1], **Padma Pradeepa Srinivasan**[2,3], **Daniel R. Zakheim**[2], **Daniel A. Harrington**[4,7], **Robert L. Witt**[2,6], **Mary C. Farach-Carson**[2,4,7], **Xinqiao Jia**[1,2,5,*], and **Swati Pradhan-Bhatt**[2,3,5,*]

[1]Department of Materials Sciences and Engineering, University of Delaware, Newark, DE

[2]Department of Biological Sciences, University of Delaware, Newark, DE

[3]Center for Translational Cancer Research, Helen F. Graham Cancer Center & Research Institute, Newark, DE

[4]BioSciences, Rice University, Houston, TX

[5]Department of Biomedical Engineering, University of Delaware, Newark, DE

[6]Otolaryngology – Head & Neck Surgery, Thomas Jefferson University, Philadelphia, PA

[7]Diagnostic and Biomedical Sciences, University of Texas Health Science Center at Houston School of Dentistry, Houston, TX

## Abstract

Myoepithelial cells are flat, stellate cells present in exocrine tissues including the salivary glands. While myoepithelial cells have been studied extensively in mammary and lacrimal gland tissues, less is known of the function of myoepithelial cells derived from human salivary glands. Several groups have isolated tumorigenic myoepithelial cells from cancer specimens, however, only one report has demonstrated isolation of normal human salivary myoepithelial cells needed for use in salivary gland tissue engineering applications. Establishing a functional organoid model consisting of myoepithelial and secretory acinar cells is therefore necessary for understanding the coordinated action of these two cell types in unidirectional fluid secretion. Here, we developed a bottom-up approach for generating salivary gland microtissues using primary human salivary myoepithelial cells (hSMECs) and stem/progenitor cells (hS/PCs) isolated from normal salivary gland tissues. Phenotypic characterization of isolated hSMECs confirmed that a myoepithelial cell phenotype consistent with that from other exocrine tissues was maintained over multiple passages of tissue culture. Additionally, hSMECs secreted basement membrane proteins, expressed adrenergic and cholinergic neurotransmitter receptors, and released intracellular calcium [$Ca^{2+}_i$] in

*To whom correspondence should be addressed: Swati Pradhan-Bhatt, Ph.D., Center for Translational Cancer Research, Suite 4300, Helen F. Graham Cancer Center & Research Institute, Christiana Care Health Systems, Newark, DE, 19713, USA. Phone: 302-623-4649, Fax: 302-623-4314, swati@udel.edu. Xinqiao Jia, Ph.D., Department of Materials Science and Engineering, University of Delaware, Newark, DE, 19716, USA. Phone: 302-831-6553, Fax: 302-831-4545, xjia@udel.edu.

response to parasympathetic agonists. In a collagen I contractility assay, activation of contractile machinery was observed in isolated hSMECs treated with parasympathetic agonists. Recombination of hSMECs with assembled hS/PC spheroids in a microwell system was used to create microtissues resembling secretory complexes of the salivary gland. We conclude that the engineered salivary gland microtissue complexes provide a physiologically relevant model for both mechanistic studies and as a building block for the successful engineering of the salivary gland for restoration of salivary function in patients suffering from hyposalivation.

**Keywords**

salivary glands; myoepithelial cells; stem/progenitor cells; spheroids; self-assembly; microtissues

## 1. INTRODUCTION

Radiation-induced hyposalivation is characterized by severe dry mouth/xerostomia, dysphagia, dysphonia, increased incidence of oral infections and an overall reduced quality of life.[1] While current treatment modalities are palliative and short-lived,[2] restoration of salivary gland function using autologous cell-derived therapies can effectively restore quality of life for head and neck cancer survivors who have undergone radiation therapy. Our long-term goal is to engineer a functional, three-dimensional salivary gland for autologous implantation in patients suffering from xerostomia.[3]

The salivary secretory complex is composed of two major cell types: acinar and myoepithelial cells, whose products are carried through an elaborate ductal network to the oral cavity. Although they are the least studied salivary cell type, myoepithelial cells are essential for glandular function and secretion in exocrine tissues. Situated between the acinar epithelium and the basement membrane, human salivary gland myoepithelial cells (hSMECs) are characterized by their dual epithelial and smooth muscle-associated expression profile.[4] This unique proteome comprises smooth muscle cytoskeletal elements and contractile machinery (α-smooth muscle actin: α-SMA; smooth muscle myosin heavy chain: SMMHC) as well as epithelial cytokeratins (e.g. KRT14 and KRT5) and adhesion molecules (EpCAM). Myoepithelial cells form desmosomal adhesions,[5] cadherins [6] and gap junctions [7] with the gland's secretory acinar cells and mediate attachment of the acinar assembly to the basement membrane through hemidesmosomes and specific integrin isoforms. The myoepithelium also aids in the synthesis and deposition of the basement membrane, upon which epithelial cells anchor and polarize. In tissue, myoepithelial cells perform diverse functional roles, best studied in mammary glands where robust contraction of the mammary alveolus in response to oxytocin has been documented.[8] Myoepithelial cells also play an integral role in establishment and maintenance of luminal cell apicobasal polarity.[9] Abundant cell-cell and cell-matrix adhesions in the myoepithelium support their role in maintaining proper tissue architecture during fluid production and secretion.[10]

To build a salivary gland tissue model from the bottom up, it is necessary to isolate and characterize the constituent cell populations. We have previously isolated and expanded hS/PCs,[11] confirmed their expression of stem/progenitor markers,[12] encapsulated them as

dispersed single cells hyaluronic acid (HA)-based hydrogels[13], investigated the role of hydrogel properties on the formation of hS/PC spheroid,[14] and differentiated them to acinar cells using neurotransmitters.[12] Separately, consistent isolation, immunophenotypic characterization and functional analyses of hSMECs are essential for the generation of *in vitro* models with lobular cells. With the two types of cells in hand, a flexible, high-throughput 3D culture platform is desirable for the organization of the respective cell types in a well-defined spatial manner.[15] Finally, the complex assemblies should be encapsulated in a permissive and instructive hydrogel matrix that approximates the properties of the connective tissue mesenchyme surrounding the salivary gland. In such heterocellular organoid models, hSMECs should enable the exchange of paracrine and juxtacrine signals, contributing to the proper function of the salivary gland.[16] In this regard, HA-based hydrogels are particularly attractive as they can be tailored to represent the biochemical and physical characteristic of the desired tissue.[3, 17]

In this study, we first describe the successful isolation of hSMECs from human salivary tissue explants. We showed the characteristic resemblance of isolated cells with the myoepithelial cells in the native salivary gland tissue and analyzed the contractile function *in vitro*. Using a hydrogel replicated microwell plate, we assembled 3D tissue-mimicking modules consisting of hS/PC spheroids with hSMECs wrapped around them. The modular co-assemblies were further encapsulated in an HA-based hydrogel to probe the function of hSMECs in a physiological relevant *in vitro* model. Our study showed, for the first time, the successful *in vitro* assembly of a salivary gland microtissue model that is reminiscent of the cellular organization of native salivary acini, providing a reliable platform to investigate myoepithelial cell biology *in vitro*.

## 2. MATERIALS AND METHODS

### 2.1. Isolation and culture of hSMECs

Healthy human salivary gland tissues for hSMEC isolation were procured from consented patients undergoing surgery for head and neck tumors following a protocol approved by Institutional Review Board (IRB) at both Christiana Care Health Systems and the University of Delaware. Any remnant connective tissue pieces were removed during the disinfecting and mincing stage. Thus, the resected parotid salivary gland tissue was predominantly epithelial in nature, largely free of stromal contaminants. A protocol for isolating hSMECs was adapted from work by Ohtomo et al. for the lacrimal gland and optimized for hSMECs.[18] Tissues were washed for 5 min in 1% (v/v) Betadine solution in DMEM/F12 (Life Technologies, Frederick, MD) and rinsed in DMEM/F12 for 2 min. The tissue was minced to a slurry, incubated at 37°C in 0.1% (w/v) collagenase I (Thermo Fisher, Barnsted, NH) in Hank's Balanced Salt Solution (HBSS) for 20 min and then centrifuged at 1,400 rpm for 3 min. The digestion process was repeated on the minced tissue, and the collected cells were added to cells from the first digest. The supernatant was strained through a 70 μm cell strainer, spun down at 1,700 rpm for 4 min, and the pellet was re-suspended in 7 mL hSMEC media [RPMI media with 10% fetal bovine serum (FBS) and 1% Penicillin/Streptomycin] and plated into a T-25 cell culture flask. Cells were grown under standard 37°C, 5% $CO_2$, 95% relative humidity conditions, and complete hSMEC media was replenished every 2

days. Following the repeat digest, only a few cells were observed in culture (Figure S1A). As the media was replenished, floating cells were discarded and attached cells proliferated. Upon reaching 60% confluence after 30 days of incubation (Figure S1B), hSMECs were trypsinized using 0.05% (w/v) trypsin-EDTA (Thermo Fisher) and neutralized with complete hSMEC media containing 10 % FBS. Passages 2 through 9 were used for throughout the study.

### 2.2. Isolation and culture of hS/PCs

Human salivary gland stem/progenitor cells (hS/PCs) were separately isolated following our previously published protocol.[12] Briefly, human parotid gland tissue was disinfected using 1% (v/v) Betadine solution in DMEM/F12, followed by mincing into a slurry in complete HepatoSTIM media (Corning Inc., Corning, NY). After reaching 70–80 % confluence, cells were trypsinized using 0.05% trypsin/EDTA, neutralized by equal volume of Soybean Trypsin Inhibitor (ATCC, Manassas, VA) and subcultured into a new flask in complete HepatoSTIM media. Passages 2 through 15 were used for this study.

### 2.3. Quantitative PCR (qPCR)

RNA was isolated from cultured hSMECs and human foreskin fibroblasts (hFF, ATCC, Manassas, VA) using the RNAeasy® mini kit (Qiagen, Valencia, CA) and DNAse treatment (Turbo DNAfree, Ambion Inc., Austin, TX). The mRNA concentration was measured using a spectrophotometer, and 1 μg mRNA was used for cDNA synthesis (cDNA synthesis kit, BioRad, Hercules, CA). The qPCR reaction was set up by mixing 12.5 μl of 2X SYBR Green mix, 5 μl forward and reverse primers, 0.5 μl of cDNA and 7.5 μl of water for each sample. Primer sequences for the genes used in this study are listed in Table 1. PCR reactions were run in two biological repeats and in triplicates, using the ABI 7300 PCR system (Life Technologies). The obtained $C_T$ values were normalized to the housekeeping gene GAPDH using $\Delta C_T$ method.[19, 20]

### 2.4. Immunostaining of tissue samples and 2D hSMEC culture

Human parotid gland cryosections (8-μm thick) fixated on positively charged glass slides (Thermo Fisher Scientific) or cells plated in 8-well NUNC chamber slides (Lab-tek® Products, Nalgene Nunc International, Naperville, IL) were fixed in 4% (v/v) paraformaldehyde (Sigma Aldrich, St Louis, MO) in phosphate buffered saline (PBS) for 10 min, washed in 1x PBS for rehydration and permeabilized for 15 min at room temperature using 0.2% (v/v) Triton X before overnight blocking with 3% (w/v) bovine serum albumin (BSA) in PBS at 4°C. On the followin g day, samples were incubated with the primary antibodies against alpha smooth muscle actin (α-SMA), smooth muscle myosin heavy chain (SMMHC), cytokeratin 14 (K14), epithelial cellular adhesion molecule (epCAM), perlecan heparan sulfate proteoglycan (perlecan/HSPG2), laminin I, collagen IV, M3 muscarinic acetylcholine receptor (M3 mAChR) or β2 adrenergic receptors for 45 min at 37°C on a rotating platform. Vendor, item n umber and the working dilution for each primary antibody were listed in Table S1. After washing three times with 1X PBS for 10 min each, a secondary antibody conjugated to AlexaFluor 488 or AlexaFluor 568 fluorophores (Life Technologies) and Draq 5 (Biostatus, Leicestershire, UK) was added and samples were incubated for 45 min at 37°C on a rotating platform. After rinsing three times in 1X PBS,

Fluoro-gel™ (Electron Microscopy Sciences, Hatfield, PA) was added and samples were stored at 4°C in the dark until confocal imaging (ZEISS, Pleasanton, CA).

### 2.5. Collagen gel contraction assay

hSMECs or hS/PCs were suspended at a density of $3 \times 10^5$ cells/ml in a collagen I solution (Corning Inc.) (3 mg/mL) at 4°C, and aliquots of 200 μl of cell suspension were added to BSA-coated wells of a 24-well plate (Cell Treat, Pepperell, MA). Samples were incubated at 37°C for 30 min before the addition of 500 μl FBS-free RPMI cell culture media. Cells were allowed to spread in the collagen gel overnight before the initiation of contraction with the addition of FBS. After 16 h of incubation at 37°C, the cell culture media was changed with the same media supplied with 10% FBS, and images of the gels were taken at 0 min. Gels were then photographed at indicated time points, and the average gel diameter for each experimental group (n=8) was calculated. Following the completion of the experiments, collagen gels immediately fixed using 4% paraformaldehyde for 30 min and followed by three PBS washes. The collagen gels were subsequently treated with the permeabilization solution (PBS containing 0.1% TritonX-100) for 45 min, stained with AlexaFluor 568-conjugated phalloidin and DAPI (Thermo Fisher) for 1 h and 30 min, respectively. After multiple PBS washes. samples were imaged with ZEISS LSM 880 (ZEISS, Pleasanton, CA) confocal microscope under fluorescence and differential reflectance modes to visualize collagen fibril, cytoskeleton and nuclei.

### 2.6. Formation of hS/PC spheroids

hS/PC spheroids were assembled in hydrogel-replicated microwells of a commercial 3D PetriDish (Sigma Aldrich). Prior to cell seeding, molds were autoclaved with a dry cycle for 15 min at 121°C. After cooling to room temperature, molds were transferred into the laminar flow hood, and a sterile solution of 2% w/v agarose (Thermo Scientific) in 0.9% (w/v) NaCl in water was prepared by heating in a microwave oven. The agarose solution was pipetted into the molds, and the gels were allowed to solidify at room temperature for 10 min. Following gelation, the hydrogel molds were transferred carefully into individual wells of a 24-well plate. This process was repeated until sufficient molds were generated. The molds then were sterilized by briefly immersing in 70% ethanol (VWR, Bridgeport, NJ), followed by 2 washes with culture media and were placed inside the laminar flow hood under UV overnight for complete sterilization. The next day, media was aspirated from the microwells and hS/PC cell suspension in HepatoSTIM media was slowly added to each well. The cell number was adjusted to achieve the desired spheroid diameter (1,440 cells/ 75 μl for 50 μm, 12,000 cells/ 75 μl for 100 μm, 40,000 cells/ 75 μl for 150 μm). Cells were allowed to settle for about 15 min inside the culture incubator, after which 1 ml of HepatoSTIM™ media containing 200 μg/ml soluble growth factor reduced mouse basement membrane extract (Corning Inc.) was immediately transferred into the well. Seeded cells were cultured at 37°C at the indicated times. Culture media was exchanged every other day.

### 2.7. Co-culture of hSMECs with hS/PC spheroids

hS/PC spheroids with a diameter of 100 μm were used for the co-culture experiments. Prior to cell seeding for co-culture studies, confluent hSMECs were trypsinized using 0.25% trypsin/EDTA for 5–8 min and were immediately neutralized using an RPMI media

containing 10% FBS and 1% Penn/Strep. After a homogenous cell suspension was achieved, cells were centrifuged at 1,000 rpm for 4 min, and the supernatant containing FBS was aspirated. The cell pellet was washed with serum-free DMEMF12 twice, and cells were resuspended in the same media. The outer membranes of hSMEC were stained with PKH26 (Sigma Aldrich), following the manufacturer's instructions. The stained hSMECs were washed twice with RPMI containing 10% FBS, before being added to hS/PC spheroids. To identify the best conditions that lead to wrapping of each spheroid by hSMECs, a concentrated hSMEC suspension (500,000 cells/ml) was prepared and serial dilution was made to achieve accurate counting of cells in each suspension added to the microwells. The number of hSMECs added was then normalized to the diameter of the spheroids. Five hSMECs/120 μm diameter spheroid were found to be optimal to achieve full coverage of the spheroid surface without overlayering. hSMEC suspensions (75 μl) with the desired cell concentration were added to the seeding chamber containing compact hS/PC spheroids. The mixture was maintained at room temperature for 15 min for hSMECs to homogenously settle on the individual hS/PC spheroid inside each microwell. Subsequently, 1 ml of HepatoSTIM media was added, and the plates were returned to the incubator for overnight culture at 37°C.

### 2.8. Hydrogel preparation and characterization

HA (500 kDa, sodium salt) was generously donated by Sanofi/Genzyme Corporation (Cambridge, MA), and thiolated HA (HA-SH, 40% modification) was prepared according our established procedure.[14] PEG (3,500 Da) bismaleimide (PEGDMI) was purchased from JenKem Technology USA (Plano, TX). Upon completion of the synthesis of HA-SH, [14, 21] the thoroughly dialyzed HA-SH solution was sterile filtered (0.22 μm) before lyophilization, and PEGDMI dissolved in PBS was sterile filtered before being used for cell culture purposes. The viscoelastic properties of HA/PEG gels were analyzed using a TA instruments DHR-3 rheometer with a 12 mm stainless steel geometry and 500 mm gap size at 37°C. Time sweep was performed with 0. 1% strain at 1 Hz. Immediately after HA-SH and PEGDMI were mixed, the mixture was loaded on a parallel plate geometry, and mineral oil was applied around the plates to prevent water evaporation. Measurement was conducted in triplicates and the average storage (G') and loss (G'') moduli were reported.

### 2.9. Hydrogel encapsulation of microtissues

After the microtissues were maintained in the microwells overnight, the agarose hydrogel replicas containing the microtissues were turned upside down inside the wells of a 24-well plate. The plate was subsequently centrifuged at 500 rpm for 5 min to recover the microtissues from the microwells. After centrifugation, the contents of every 4 wells of a 24-well plate were transferred to a 1.5 ml centrifuge tube and were spun at 500 rpm for 3 min. The microtissue pellet was first resuspended in 200 μl of 1% (w/v) HA-SH and mixed with 1% (w/v) PEGDMI at a 1:1 (v/v) ratio in a cell culture insert. Gelation occurred immediately after PEGDMI was added. HepatoSTIM media (300 μl) was added on top of each gel, and additional 500 μl media was added around the culture insert. Fluorescent labeling and further staining of microtissues were performed as follows. First, hSMECs were labeled with PKH26 cell membrane live cell dye prior to forming microtissues. Hydrogel encapsulated microtissues first were washed with warm PBS and then fixed with 4% paraformaldehyde in

PBS for 30 min. After three brief washes with 1X PBS (1–2 min each), the constructs were transferred to an 8-well Nunc chamber (Thermo Scientific) and were treated with 0.1 % Triton-X 100 for another 30 min. DAPI diluted in PBS was subsequently added, and the constructs were incubated for 30 min before being subjected to rigorous PBS washes. Confocal imaging was performed with a ZEISS LSM710 inverted confocal microscope (ZEISS, Pleasanton, CA). Collected Z-stacks were further deconvoluted to achieve maximum-intensity projection images of different sections of the hydrogel using ZEN Software (ZEISS ZEN, Peabody, MA).

### 2.10. Immunostaining of microtissues

hS/PC spheroids were embedded in Tissue-Tek OCT-compound (vWR, Philadelphia, PA) and 10 um sections were sliced using a Leica 3050 cryostat (Leica Systems, BuffaloGrove, IL). Sectioned slices were affixed onto a Leica CryoJane microscope slide (Leica Systems) and the immunostaining protocol described in section 2.4 were followed. Separately, hydrogel encapsulated microtissues or hS/PC spheroids were fixed in 4% (v/v) paraformaldehyde (Sigma Aldrich, St Louis, MO) in PBS for 30 min, washed in 1X PBS, and permeabilized and blocked with 2% BSA and 0.1% TX100 in 1X PBS for 2 h. Next, samples were incubated with the primary antibody against alpha ki67 (Table S1) overnight at 4°C. After washing three times with 1 × PBS for 15 min each, a secondary antibody conjugated to AlexaFluor 488 or AlexaFluor 568 fluorophores (Life Technologies) and DAPI were added. Samples were incubated for 90 min at room temperature, followed by washing three times with 1X PBS for 15 min each. Finally, samples were first incubated with Alexa Fluor 488 Phalloidin (Life Technologies) for 30 min, and subsequently with DAPI (Thermo Fischer) for 15 min. After a final wash with 1X PBS (3 times, 15 min each), samples were immediately imaged with a ZEISS LSM710 inverted confocal microscope.

### 2.11. Intracellular calcium ($[Ca^{2+}_i]$) imaging

Fluo4 AM NW fluorescent calcium indicator (Life Technologies) was used to detect the intracellular baseline and agonist-induced $[Ca^{2+}_i]$ levels in hSMECs. For 2D calcium imaging, 10,000 hSMECs were plated in a 8-well nunc chamber and were incubated overnight in RPMI media containing 10% FBS. On the day of the experiment, Fluo4 AM NW solution was freshly prepared by dissolving the dye powder in 10 ml HEPES buffer containing 100 μl probenecid solution provided by the supplier. Next, the culture media was replaced with 250 μl of Fluo4 AM NW solution, and the cultures were maintained at 37°C for at least 45 min to allow the dye to diffuse into the cells. To detect changes in $[Ca^{2+}_i]$ levels, thapsigargin (20 μM, Sigma Aldrich) and carbachol (CCh, 200 μM, Sigma Aldrich) were added to media over the cultures and agonist-induced intracellular $[Ca^{2+}_i]$ levels were imaged by confocal microscope using a 488 nm argon laser source (Ex: 494 nm; Em: 516 nm). Once the calcium signal was detected, the live cell imaging setup was configured to record the fluorescent signal until the $[Ca^{2+}_i]$ fluorescent signal was quenched. Variations in the resting fluorescence values across samples were taken into account by subtracting the background values from each data point. Results were expressed as relative fluorescence unit (RFU) as a function of time. To detect $[Ca^{2+}_i]$ in 3D microtissues, hSMECs were labeled with Cell Tracker Red™ (Life Technologies) before seeding onto the hS/PC spheroids in order to distinguish hSMECs from hS/PCs. Hydrogels containing microtissues

were transferred to an 8-well Nunc chamber containing 250 μl Fluo4 AM NW dye solution and were incubated for 60–90 min at 37°C. The 3D salivary gland microtissues were analyzed for calcium signals following the same protocol described above for 2D hSMEC cultures.

### 2.12. Statistical analysis

All quantitative measurements were performed using three replicate samples. Statistical significance was evaluated using ANOVA. A $p$ value of less than 0.05 was considered as statistically significant.

## 3. RESULTS

This study aimed to reconstitute isolated hS/PCs and hSMECs into a multicellular microtissue that mimics the basic cellular organization of salivary gland secretory acini.

### 3.1. Phenotypic characterization of isolated hSMECs

Cells from primary explants were examined over four weeks of culture to assess the morphology of the isolated cells. Initially fewer than ten cells attached to the T25 culture flask after repeated enzymatic digestion at Day 1, and this pure population of cells was expanded until they reached 60% confluency (Figure S1). Figure 1A(ii) shows that the selective culture conditions produced and supported growth of cells with an elongated, spindle shaped morphology. Expression of myoepithelial cell markers was examined using immunofluorescence and specific antibodies (Figure 1B). Markers that selectively stained the myoepithelium include the smooth muscle myosin heavy chain (SMMHC), cytokeratin 14 (K14) and α-smooth muscle actin (α-SMA). The tissue sections (Figure 1B, i-iii) revealed the peripheral localization of myoepithelial cells around the acini in the native tissue. Isolated hSMECs were stained positive for SMMHC, K14 and α-SMA (Figure 1B, iv-vi), confirming their myoepithelial phenotype. In addition, isolated hSMECs did not express acinar (AQP-5) or ductal (K19) markers, as confirmed by immunostaining (Figure S2).

In order to assess the location and composition of the basement membrane, we first immunolabeled the tissue sections for characteristic basement membrane proteins: perlecan, collagen type IV, laminin (Figure 1C, i-iii). Further staining of hSMECs for the basement membrane proteins showed that hSMECs have high expression levels for key basement membrane proteins (Figure 1C, iv-vi). Comparison of the expression levels of transcripts encoding myoepithelial markers in hSMECs and in hFFs confirms the epithelial nature of isolated hSMECs. As seen in Figure 1D, isolated hSMECs expressed transcripts for all myoepithelial-specific markers,[22] including cytokeratin 14 (KRT14), cytokeratin 5 (KRT5), myosin heavy chain 11 (MYC11) and smooth muscle actin (ACTA2), whereas hFF only expressed transcripts for MYC11 and ACTA2. Transcripts encoding epithelial specific markers KRT14 and KRT5 were undetectable in hFF. In addition, no significant differences in myoepithelial-specific transcripts were noted for hSMECs at early passages (P2-P4) when compared to late passages (P7-P9, Figure 1D).

### 3.2. Expression of neurotransmitter receptors and response to muscarinic agonists by hSMECs

To evaluate the function of myoepithelial cells, the presence of neurotransmitter receptors and their activation by the addition of adrenergic and cholinergic agonists were analyzed. Isolated hSMECs expressed $\beta_2$-adrenergic (Figure 2A) and $M_3$ muscarinic (Figure 2B) neurotransmitter receptors on their membranes, which were readily detected by specific immunostaining. To assess the ability of hSMECs to store and release $[Ca^{2+}_i]$ in response to CCh (Figure 2C, D), we investigated the activation of the cholinergic pathway in hSMECs. Initially, a test experiment using thapsigargin was performed to confirm the experimental protocols (Figure S3). After CCh was introduced, a sharp spike in $[Ca^{2+}_i]$ signal was observed in CCh-responsive hSMEC cells (Figure 2D). The normalized initial $[Ca^{2+}_i]$ signal was measured to be approximately 50 RFU, while after stimulation with CCh, the $[Ca^{2+}_i]$ signal spiked up to 1700 RFU and almost immediately returned back to baseline levels after ~100 s. It should be noted that not all cells responded to CCh stimulation. The normalized RFU for unresponsive cells (Figure 2D, black line) was close to the baseline level. These results confirmed that isolated hSMECs could respond to neurotransmitter agonists as is expected of semi-excitable cells.

### 3.3. Contractility of hSMECs in collagen gels

hSMECs were grown in type I collagen gels to investigate cellular contractility. Imaging the constructs under fluorescence and reflectance modes permits a direct assessment of cellular interaction with collagen fibrils during the contraction assay. hSMECs spread readily in collagen gels and contracted collagen fibrils, as seen by light grey tractions concentrated around the cell bodies (white arrows, Figure 3A). On the other hand, hS/PCs only formed small protrusions around the cell periphery and no obvious reorganization of collagen fibrils was observed (Figure 3B). Analysis of the gel diameter as a function of time (Figure 3C) further confirmed the distinctly different contractile properties between hSMECs and hS/PCs. Within 6 h after being placed in FBS containing media, hSMECs contracted collagen gels to 80% of their initial diameter, whereas addition of hS/PCs to gels only reduced the original diameter to 90%. By the 48-h time point when the experiment was terminated, no further gel contraction was seen for the gels containing hS/PCs. Consistent with their function as contractile cells, hSMECs reduced the diameter of collagen gels to 60% of their initial diameter over this period. Figure 3D shows the images of the gels at times 0 and 48 h containing either hS/PCs or hSMECs.

### 3.4. Formation of hS/PC spheroids

To further assess the functions of hSMECs, we developed a tissue-mimetic co-culture platform consisting of an hS/PC spheroid encased by hSMECs. Our method started with replicating the microwell mold (300 μm × 800 μm) with non-adhesive, agarose gel (Figure 4A), followed by forming condensed hS/PC spheroids in hydrogel microwells (Figure 4B). Cells introduced to the microwells formed spheroids of consistent sizes with high reproducibility. Next, dispersed hSMECs were seeded onto hS/PC spheroids and were allowed to assemble over the spheroids to establish close cell-cell contact (Figure 4B). The

resulting co-cultures were collected from the microwells and processed for further investigation of hSMEC biology in 3D.

Following the initial cell seeding, compact hS/PC spheroids of varying diameters were obtained after 7 days of culture in the agarose microwells in the presence of soluble basement membrane extract (Figure 5A). The average diameter of hS/PC spheroids correlated with the cell seeding density per well (Figure 5B). At a seeding density of 15, 125 or 416 cells/well, structures with an average diameter of 31.0 ± 3.5, 58.8 ± 7.1 and 129.7 ± 12.5 μm were obtained, respectively. Microwell-grown hS/PC spheroids were examined for their morphology and cytoskeletal organization (Figure 5 C). Figure 5C i showed that cells were tightly packed within each structure and individual structures exhibited a distinct boundary at the outer surface of the spheroid. Figure 5C ii showed that individual cells within the spheroids were separated by cortical actin structures. When the spheroids were cryosectioned, the presence of a central lumen often was observed (Figure 5C iii). Immunostaining of hS/PC spheroids for a cell proliferation marker, Ki67, revealed the presence of proliferative cells (Figure 5C iv) within the structure.

### 3.5. Formation of salivary gland microtissues

After hS/PCs formed compact spheroids in the microwells, dispersed hSMECs were seeded at an optimized 5 hSMEC/ hS/PC spheroid ratio. Figure 6A shows microscopic images of the microtissue at different stages of development. After the initial seeding, hS/PCs loosely aggregated in the microwell (Figure 6Ai). By day 5, compact hS/PC spheroids were obtained (Figure 6Aii). The presence of fluorescently-labeled hSMECs covering individual hS/PC spheroids were evident under the combined phase contrast-fluorescent mode (Figure 6Aiii, iv). When 2 hSMECs were added to each well, individual hS/PC spheroids were sparsely decorated by hSMECs. A full coverage of the spheroid structure was achieved at higher hSMEC loading concentrations (5 hSMEC/well).

The assembled structures were encapsulated in an HA gel crosslinked by PEGDMI. Gelation occurred immediately after mixing of HA-SH and PEGDMI and reached a storage modulus (G') of 43 ± 18 Pa and a loss modulus (G") of 0.5 ± 0.1 Pa 3 h (10,800 s) post-mixing (Figure 6B). Confocal imaging of hydrogel containing encapsulated co-cultures (Figure 6C) revealed the presence of hSMECs (stained purple by PKH26) on the outer surface of the DAPI-stained hS/PC spheroids in the co-culture. Figure 6D shows a high magnification image with different cross-sectional views, confirming the spatial arrangement of hSMECs within the microtissue assemblies in the HA gel.

### 3.6. hSMEC contractility and agonist-induced [$Ca^{2+}_i$] response from hydrogel encapsulated microtissues

Using the biomimetic hydrogel co-culture platform, we examined agonist-induced coordinated calcium activation throughout the microtissues. A tile scan from confocal live cell imaging (Figure 7A) demonstrated changes in [$Ca^{2+}_i$] levels of CCh-treated microtissues containing both hS/PCs and hSMECs. hSMECs were labeled with CTR (red) in order to distinguish them from hS/PCs. The heatmap profile in each panel (i-iv) shows successive oscillations in [$Ca^{2+}_i$] intensities observed at 1 min 6 s, 2 min 2 s and 4 min 36 s

post CCh treatment. Moreover, [$Ca^{2+}_i$] oscillations were observed at the periphery of each microtissue structure, suggestions that such responses were predominately from hSMECs. Figure 7B shows a representative plot of a single cell undergoing oscillations. Overall, the assembled microtissues responded to neurotransmitter stimulation in a coordinated fashion (Video S1). We further analyzed the contractility of hSMECs within the microtissue structure by tracking the cytoskeletal movements during live cell imaging (Video S2). Our result showed continuous remodeling of actin cytoskeleton of hSMECs encasing the hS/PC spheroids at the resting state.

## 4. DISCUSSION

Salivary gland secretory function necessitates the concerted actions of acinar, ductal and myoepithelial cells. The unique rearrangement of these cells in this highly branched organ terminating in secretory end buds enables the vectorial transport of saliva. Towards bioengineering complex glandular models[11, 23], we previously reported the isolation and phenotypic characterization of hS/PCs, as confirmed by the expression of progenitor markers (K5, K14, MYC, ETV4, ETV5) and the ability of hS/PCs in hydrogels to differentiate into a specialized acini-like cell type upon neurotransmitter stimulation.[12] Our custom-designed HA hydrogels promoted spheroid assembly from dispersed hS/PCs.[14] We further discovered that hS/PCs cultured in HA gels decorated with bioactive peptides expressed a significantly higher levels of progenitor markers as compared to the unmodified HA gels.[12] The current study aimed to create physiologically relevant microtissues composed of myoepithelial cells and organized, acini-like spheroids to replicate the function of intact acini-hSMEC assemblies in tissue. At present, there is no similar physiologically relevant *in vitro* model for providing myoepithelial cell functions, in terms of phenotype, contractility and cell-cell interactions, to engineered acini-like spheroids.

Aside from earlier work concerning *in vitro* characterization of salivary gland myoepithelial cells,[24, 25] much of what we know about myoepithelial cells is based on studies on the mammary glands. In mammary glands, myoepithelial cells are responsible for robust contraction of the mammary alveolus in response to oxytocin [8], and the contractile mechanism is similar to that observed in smooth muscle cells.[8, 26–29]. Myoepithelial cells also play an integral role in the establishment and maintenance of luminal cell apicobasal polarity [9]. Abundant cell-cell and cell-matrix adhesions in the myoepithelium support maintaining proper tissue architecture during fluid production and secretion.[10] To perform their specialized functions, myoepithelial cells express α-SMA, synthesize laminin-1, integrins, vinculin and α-actinin, [8, 30] and respond to neurotransmitter, neuropeptide, purinergic and hormone signals via specific receptors.

We successfully isolated hSMECs from human salivary gland tissues and expanded them in culture to obtain a seemingly pure population of myoepithelial cells. The isolated cells exhibited a spindle-shaped morphology and retained myoepithelial markers observed in the native salivary glands. Expression of myoepithelial cell biomarkers was maintained through at least six cell passages. Consistent with our findings, Chan et al. reported high expression of levels of α-SMA from myoepithelial cells they isolated from human parotid glands. [31]

Isolated hSMECs were contractile. It is postulated that both myoepithelial contraction and acinar cell membrane transport mechanisms contribute to salivary secretion. In mammary and lacrimal glands, the contractile function of myoepithelial cells depends upon activation of a specific subset of G protein-coupled receptors (GPCRs) [8, 26–28] that stimulates a phospholipase C-mediated pathway driving increased cytosolic calcium; a response which mirrors the conventional contractile mechanism observed in smooth muscle cells [29]. Stimulation with the cholinomimetic muscarinic receptor agonist CCh increased intracellular [$Ca^{2+}_i$] in myoepithelial cells. We hypothesized that intracellular [$Ca^{2+}_i$] release in myoepithelial cells might drive a contractile response; myoepithelial cells express similar contractile machinery to that of smooth muscle cells, whose contractility is regulated by changes in cytosolic calcium levels [32, 33]. Increased intracellular [$Ca^{2+}_i$] in smooth muscle cells and subsequent complex formation with the regulatory protein calmodulin leads to activation of myosin light chain kinase. This protein serves as the primary initiator of actomyosin crossbridge cycling during cell contraction.

The observed increase in [$Ca^{2+}_i$] upon treatment with parasympathetic agonists provided a strong rationale for designing functional assays to examine cell contraction in isolated myoepithelial cells. Thus, hSMECs were encapsulated in collagen I gels to investigate their relative contractility in comparison to salivary hS/PCs and acellular gels. Collagen gel contraction assay is a well-established method to evaluate cellular contractility. [34, 35]. When seeded in collagen I matrices, contractile cells can generate an observable shrinkage in gel diameter by remodeling the collagen fibers through forces applied during contraction. hSMECs demonstrated a robust contractile phenotype in collagen I gel assays, evidenced by their greater capacity for collagen matrix remodeling than non-contractile cells. Of note, contraction is understood to be a relatively quick process, with multiple cycles of contraction and relaxation occurring over the course of a stimulated saliva secretion [36]. Each cycle of contraction and relaxation would, in theory, further compact the collagen gel, explaining the significant shrinkage observed continuously over time.

With hSMECs fully characterized and hS/PCs already established from our previous studies, [11] we devised a bottom-up approach to produce salivary gland microtissues with a tissue-mimetic architecture. Various methods have been developed for the formation of compact organoids.[37] The traditional hanging drop technique does not allow precise control of spheroid sizes and spheroid handling and manipulation are not straightforward. Alternatively, spheroids can be produced via suspension culture using non-adhesive tissue culture plates.[38] This method suffers from poor control over cell density, spheroid size/shape and cellular organization. It does not support the establishment of *in vitro* models with a well-defined spatial arrangement of multiple cell types. Here, we used agarose gel-replicated microwells, initially developed by Morgan and colleagues, [39, 40] that restrict cells in a confined space with a defined dimension. Each replica contains 96 microwells, allowing the formation of multiple multicellular assemblies in a simple and reproducible manner. Our bottom-up assembly strategy allows efficient and rapid production of hS/PC spheroids and hS/PC-hSMEC structures in a high-throughput fashion. The resulting secretory units can be easily collected from the microwells and subsequently be encapsulated in a biomimetic hydrogel matrix for functional assessment.

In the native gland, each acinus is encased by myoepithelial cells. Thus, to further mimic the cellular composition of the native acinus, hSMECs were seeded on the preformed hS/PC spheroids to establish a similar cell ratio and to ensure complete wrapping of the spheroids by hSMECs. hSMECs co-assembled with hS/PC-derived spheroids responded to neurotransmitters in a coordinated fashion and actively remodeled their cytoskeleton during 3D co-culture. We then used a HA-based hydrogel to establish an appropriate tissue-like environment the cell assemblies to grow into. Custom-designed HA hydrogels have shown success in maintaining high viability of single hS/PCs and promoting the formation of spheroid structures *in vitro*.[13, 14] In this study, we utilized PEGDMI to crosslink HA-SH as rapid gelation is necessary to prevent the microtissue assemblies from settling. Our initial experiments showed that hSMECs remained on the outer surface of the hS/PC spheroids for up to 48 h in the HA gel without any biological signals. Given that the signaling leading to calcium release by the hSMECs could be activated by CCh stimulation, we investigated if agonist stimulation of the hSMECs can relay these signals to the hS/PC spheroids within the hSMEC-hS/PC complex. In addition to providing the correct physiological topography for the hSMECs, the hS/PC spheroids also responded to CCh stimuli, indicating that our hSMEC-hS/PC co-culture system has the potential to attain complete functionality if provided with appropriate cues.

While the current investigation provides an essential proof-of-concept step towards salivary gland tissue engineering through creation of microtissues capable of responding to neurotransmitters, we believe that the restoration of the complete secretory function by the salivary co-assemblies will require exposure to nervous tissue, a property to be tested in the next series of studies we will undertake on this important endeavor.

## 5. CONCLUSION

Towards the goal of establishing the functional secretory units of the salivary gland, myoepithelial cells were isolated from healthy human tissues and characterized morphologically, phenotypically and functionally. The isolated cells were spindle-shaped, retained myoepithelial markers seen in native tissue and exhibited contractility upon parasympathetic stimulation. A novel microwell culture system was utilized for the assembly of hS/PCs into compact spheroid structures. The addition of hSMECs to the compact hS/PC spheroids led to surface encasement of the spheroids by hSMECs, recreating the spatial arrangement of cellular components of the lobular secretory complex seen in native tissue. The salivary gland microtissue assemblies were encapsulated in a synthetic matrix derived from HA and PEGDMI. Microtissues cultured in HA gels were further assessed for agonist induced intracellular [$Ca^{2+}_i$] responses. Coordinated [$Ca^{2+}_i$] signaling between hS/PCs and hSMECs in the reconstituted salivary microtissues suggested cell-cell communication between the two cell-types. The bottom up tissue assembly can be further exploited to understand salivary gland function from a cellular/organoid perspective and to provide a new approach toward restoration of salivary functions in patients with xerostomia.

## Supplementary Material

Refer to Web version on PubMed Central for supplementary material.

## Acknowledgments

This work was supported by National Institutes of Health (NIDCR, R01 DE022969), the University of Delaware and private philanthropic donations. The authors would like to thank the Tissue Procurement Center at the Helen F. Graham Cancer Center & Research Institute and Christiana Care Health Services Inc. for procuring human salivary gland tissue for this work. We also thank Dr. Jeffrey Caplan for his expert advice on calcium imaging, Dr. Ying Hao for her assistance with rheological characterizations of the HA gels and Dr. Matthew Hoffman and all the members of the Farach-Carson/Harrington laboratories for many helpful discussions. We acknowledge Sanofi/Genzyme for generously providing HA.

## References

1. Narhi TO, Meurman JH, Ainamo A. Xerostomia and hyposalivation: causes, consequences and treatment in the elderly. Drugs Aging. 1999; 15(2):103–16. [PubMed: 10495070]
2. Villa A, Connell CL, Abati S. Diagnosis and management of xerostomia and hyposalivation. Ther Clin Risk Manag. 2015; 11:45–51. [PubMed: 25653532]
3. Ozdemir T, et al. Biomaterials-based strategies for salivary gland tissue regeneration. Biomater Sci. 2016; 4(4):592–604. [PubMed: 26878077]
4. Adriance MC, et al. Myoepithelial cells: good fences make good neighbors. Breast Cancer Res. 2005; 7(5):190–7. [PubMed: 16168137]
5. Runswick SK, et al. Desmosomal adhesion regulates epithelial morphogenesis and cell positioning. Nat Cell Biol. 2001; 3(9):823–30. [PubMed: 11533662]
6. Bissell MJ, Bilder D. Polarity determination in breast tissue: desmosomal adhesion, myoepithelial cells, and laminin 1. Breast Cancer Res. 2003; 5(2):117–9. [PubMed: 12631393]
7. Taugner R, Schiller A. Gap junctions on myoepithelial cells. Cell Tissue Res. 1980; 206(1):65–72. [PubMed: 7357595]
8. Haaksma CJ, Schwartz RJ, Tomasek JJ. Myoepithelial cell contraction and milk ejection are impaired in mammary glands of mice lacking smooth muscle alpha-actin. Biol Reprod. 2011; 85(1): 13–21. [PubMed: 21368298]
9. Gudjonsson T, et al. Normal and tumor-derived myoepithelial cells differ in their ability to interact with luminal breast epithelial cells for polarity and basement membrane deposition. J Cell Sci. 2002; 115(Pt 1):39–50. [PubMed: 11801722]
10. Glukhova M, et al. Adhesion systems in normal breast and in invasive breast carcinoma. Am J Pathol. 1995; 146(3):706–16. [PubMed: 7887451]
11. Pradhan S, et al. Perlecan domain IV peptide stimulates salivary gland cell assembly in vitro. Tissue Eng Part A. 2009; 15(11):3309–20. [PubMed: 19382872]
12. Srinivasan PP, et al. Primary Salivary Human Stem/Progenitor Cells Undergo Microenvironment-Driven Acinar-Like Differentiation in Hyaluronate Hydrogel Culture. Stem Cells Transl Med. 2017; 6(1):110–20. [PubMed: 28170182]
13. Pradhan-Bhatt S, et al. Implantable three-dimensional salivary spheroid assemblies demonstrate fluid and protein secretory responses to neurotransmitters. Tissue Eng Part A. 2013; 19(13–14): 1610–20. [PubMed: 23442148]
14. Ozdemir T, et al. Tuning Hydrogel Properties to Promote the Assembly of Salivary Gland Spheroids in 3D. ACS Biomater Sci Eng. 2016; 2(12):2217–30. [PubMed: 27990487]
15. Schell JY, et al. Harnessing cellular-derived forces in self-assembled microtissues to control the synthesis and alignment of ECM. Biomaterials. 2016; 77:120–9. [PubMed: 26610075]
16. Wan AC. Recapitulating Cell-Cell Interactions for Organoid Construction - Are Biomaterials Dispensable? Trends Biotechnol. 2016; 34(9):711–21. [PubMed: 27012157]
17. Dicker KT, et al. Hyaluronan: a simple polysaccharide with diverse biological functions. Acta Biomater. 2014; 10(4):1558–70. [PubMed: 24361428]
18. Ohtomo K, et al. Increase of intracellular Ca2+ by purinergic receptors in cultured rat lacrimal gland myoepithelial cells. Invest Ophthalmol Vis Sci. 2011; 52(13):9503–15. [PubMed: 22039237]

19. Patel VN, et al. Specific heparan sulfate structures modulate FGF10-mediated submandibular gland epithelial morphogenesis and differentiation. J Biol Chem. 2008; 283(14):9308–17. [PubMed: 18230614]
20. Srinivasan PP, et al. Injectable perlecan domain 1-hyaluronan microgels potentiate the cartilage repair effect of BMP2 in a murine model of early osteoarthritis. Biomed Mater. 2012; 7(2):024109. [PubMed: 22455987]
21. Xu X, et al. Recreating the tumor microenvironment in a bilayer, hyaluronic acid hydrogel construct for the growth of prostate cancer spheroids. Biomaterials. 2012; 33(35):9049–60. [PubMed: 22999468]
22. Daniel L, et al. Expression of Smooth Muscle-Specific Proteins in Myoepithelium and Stromal Myofibroblasts of Normal and Malignant Human Breast Tissue. Proceedings of the National Academy of Sciences of the United States of America. 1993; 90(3):999–1003. [PubMed: 8430113]
23. Nelson J, Manzella K, Baker OJ. Current cell models for bioengineering a salivary gland: a mini-review of emerging technologies. Oral Dis. 2013; 19(3):236–44. [PubMed: 22805753]
24. Redman RS. Myoepithelium of salivary glands. Microsc Res Tech. 1994; 27(1):25–45. [PubMed: 8155903]
25. Lung MA. Autonomic nervous control of myoepithelial cells and secretion in submandibular gland of anaesthetized dogs. J Physiol. 2003; 546(Pt 3):837–50. [PubMed: 12563008]
26. Dartt DA, Hodges RR. Cholinergic agonists activate P2×7 receptors to stimulate protein secretion by the rat lacrimal gland. Invest Ophthalmol Vis Sci. 2011; 52(6):3381–90. [PubMed: 21421880]
27. Hodges RR, et al. Identification of vasoactive intestinal peptide receptor subtypes in the lacrimal gland and their signal-transducing components. Invest Ophthalmol Vis Sci. 1997; 38(3):610–9. [PubMed: 9071214]
28. Satoh Y, et al. Effects of carbachol and catecholamines on ultrastructure and intracellular calcium-ion dynamics of acinar and myoepithelial cells of lacrimal glands. Cell Tissue Res. 1997; 289(3): 473–85. [PubMed: 9232826]
29. Webb RC. Smooth muscle contraction and relaxation. Adv Physiol Educ. 2003; 27(1–4):201–6. [PubMed: 14627618]
30. Deugnier MA, et al. Myoepithelial cell differentiation in the developing mammary gland: progressive acquisition of smooth muscle phenotype. Dev Dyn. 1995; 204(2):107–17. [PubMed: 8589435]
31. Chan YH, et al. Selective culture of different types of human parotid gland cells. Head Neck. 2011; 33(3):407–14. [PubMed: 20645288]
32. Beamish JA, et al. Molecular regulation of contractile smooth muscle cell phenotype: implications for vascular tissue engineering. Tissue Eng Part B Rev. 2010; 16(5):467–91. [PubMed: 20334504]
33. Pfitzer G, Arner A. Involvement of small GTPases in the regulation of smooth muscle contraction. Acta Physiol Scand. 1998; 164(4):449–56. [PubMed: 9887968]
34. Oishi K, et al. Agonist-induced isometric contraction of smooth muscle cell-populated collagen gel fiber. Am J Physiol Cell Physiol. 2000; 279(5):C1432–42. [PubMed: 11029291]
35. Souren JE, et al. Factors controlling the rhythmic contraction of collagen gels by neonatal heart cells. In Vitro Cell Dev Biol. 1992; 28A(3 Pt 1):199–204. [PubMed: 1582995]
36. Gudjonsson T, et al. Myoepithelial cells: their origin and function in breast morphogenesis and neoplasia. J Mammary Gland Biol Neoplasia. 2005; 10(3):261–72. [PubMed: 16807805]
37. Picollet-D'hahan N, et al. A 3D Toolbox to Enhance Physiological Relevance of Human Tissue Models. Trends Biotechnol. 2016; 34(9):757–69. [PubMed: 27497676]
38. Shubin AD, et al. Encapsulation of primary salivary gland cells in enzymatically degradable poly(ethylene glycol) hydrogels promotes acinar cell characteristics. Acta Biomater. 2017; 50:437–449. [PubMed: 28039063]
39. Napolitano AP, et al. Scaffold-free three-dimensional cell culture utilizing micromolded nonadhesive hydrogels. Biotechniques. 2007; 43(4):494, 496–500. [PubMed: 18019341]
40. Napolitano AP, et al. Dynamics of the self-assembly of complex cellular aggregates on micromolded nonadhesive hydrogels. Tissue Eng. 2007; 13(8):2087–94. [PubMed: 17518713]

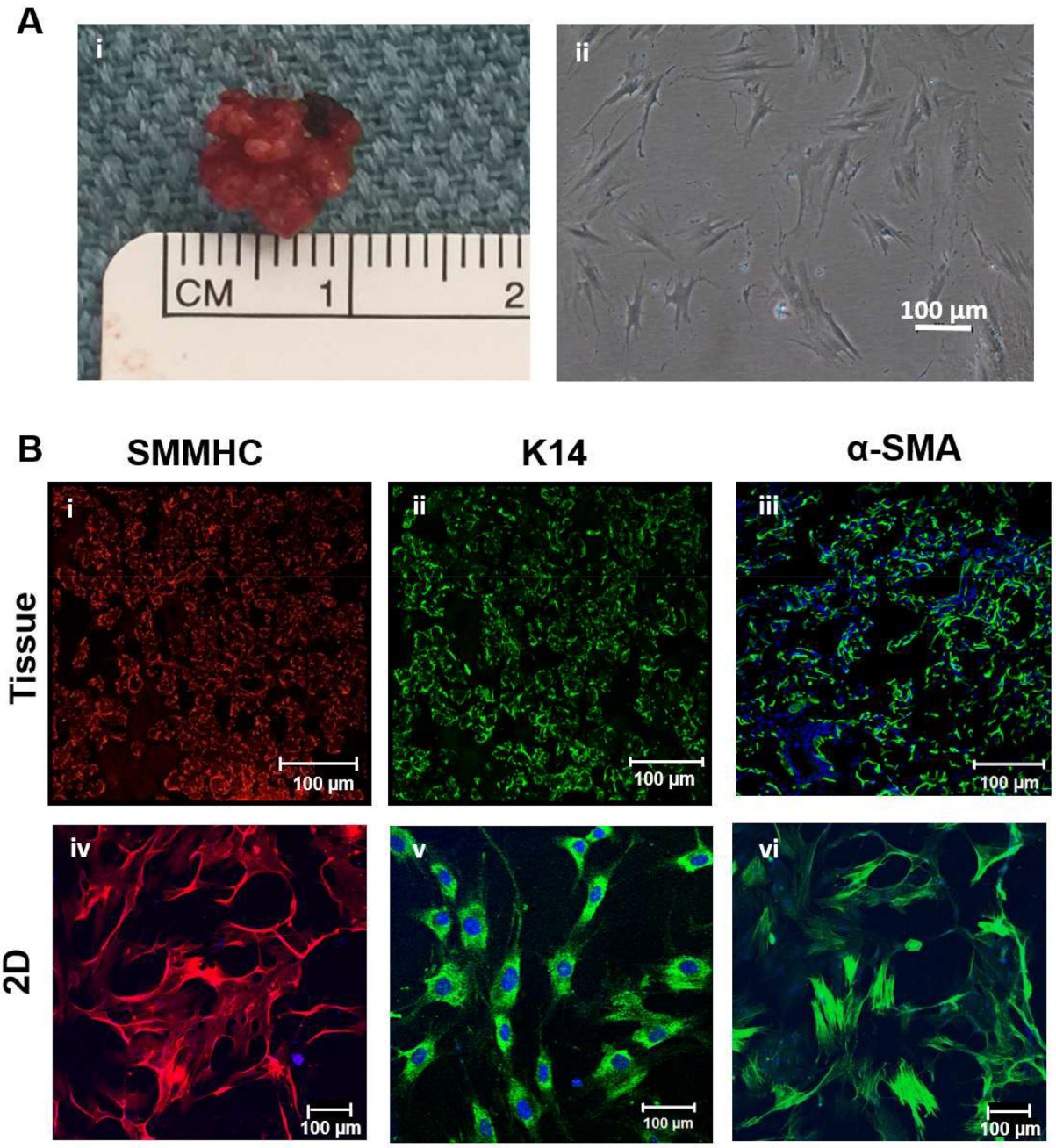

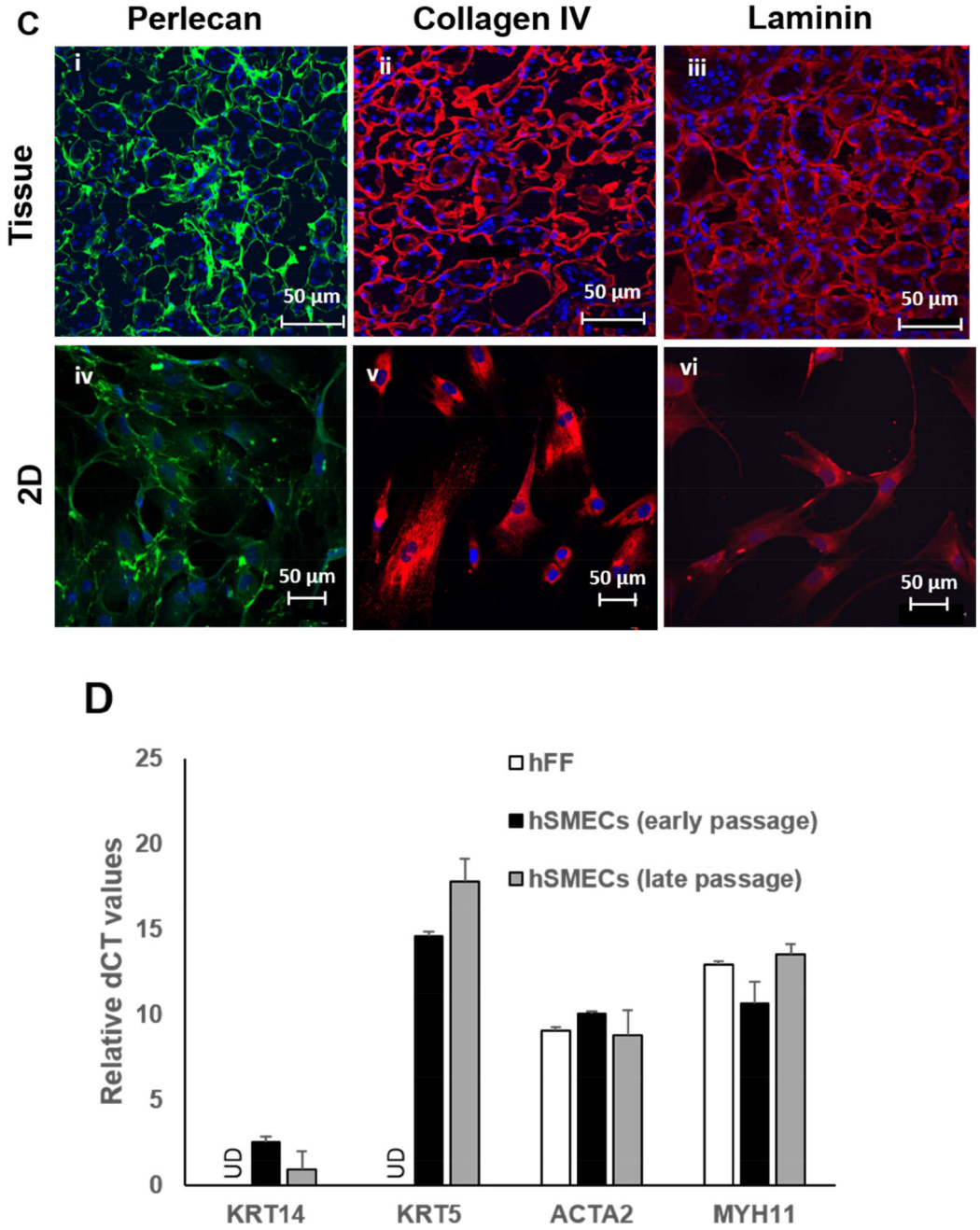


**Figure 1. Morphological and phenotypical characterization of isolated hSMECs**

**(A)**. Human salivary parotid gland tissue after resection (A, i) and human salivary myoepithelial cells after selective isolation (A, ii). **(B)**. The expression of myoepithelial cell markers was confirmed for smooth muscle myosin heavy chain (SMMHC, red, i, iv), cytokeratin 14 (K14, green, ii, v) and alpha-smooth muscle actin (α-SMA, green, iii, vi). Nuclei were counter-stained by DAPI (blue). **(C)**. Basement membrane proteins perlecan (green), collagen IV (red), laminin (red) were present in isolated hSMECs. **(D)**. The relative expression levels of myoepithelial marker KRT5, KRT14, MYH11 and ACTA2 by hSMECs

at low (P2-P4) and high (P7-P9) passage numbers were analyzed using qPCR. hFFs were included for comparison purposes. UD: Undetected.

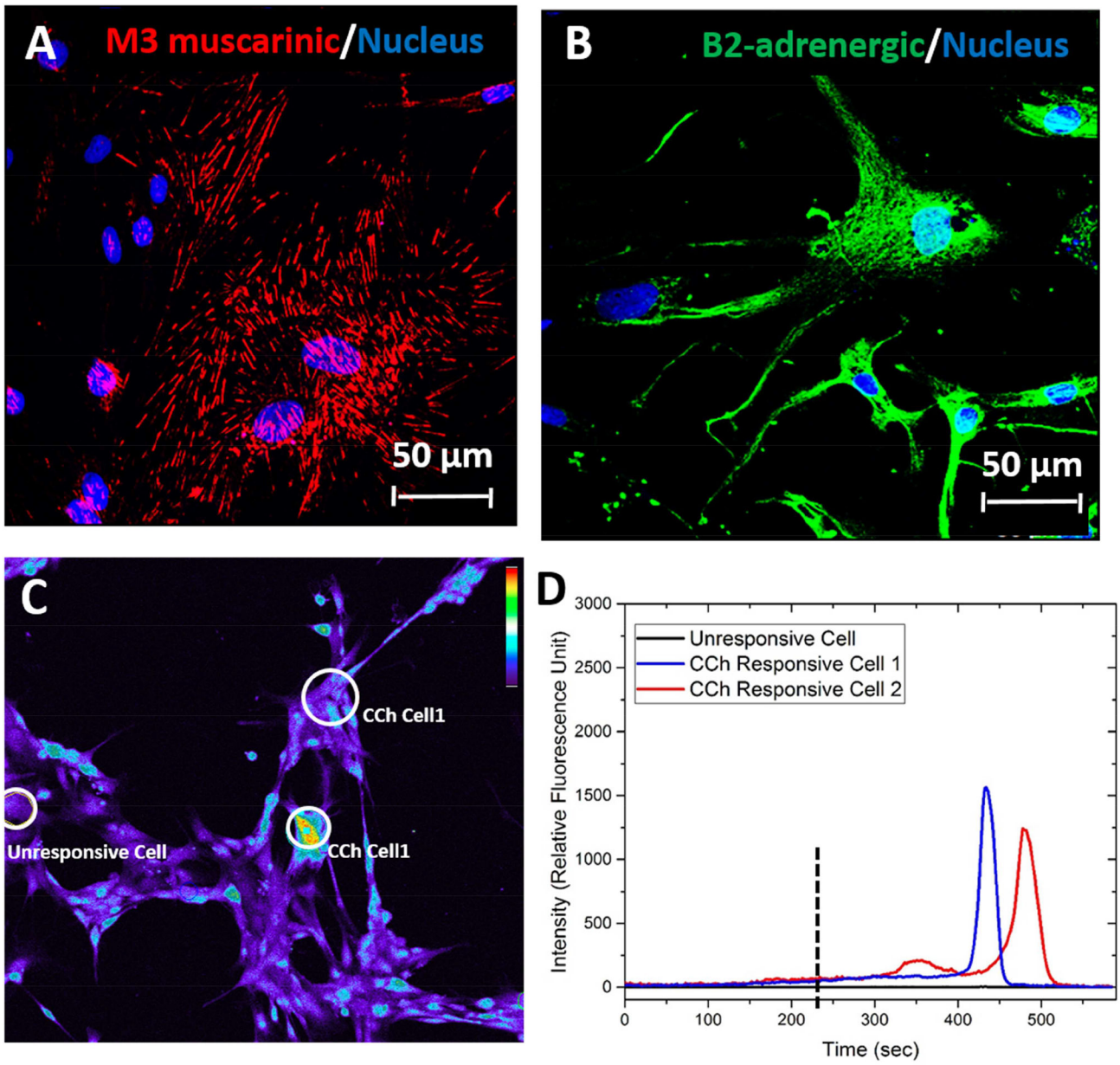


**Figure 2. Functional Responses**

Expression and localization of M3 muscarinic (**A**, red) and β2-adrenergic (**B**, green) receptors and intracellular calcium signals in hSMECs (**C, D**). The $[Ca^{2+}{}_i]$ signals were detected by treating hSMECs with M3 muscarinic acid agonist carbachol (CCh, 200 mM) and the response was observed by a subpopulation of hSMECs cultured on glass (**C**). The relative fluorescent intensity of $[Ca^{2+}{}_i]$ in response to CCh over time was plotted for CCh-responsive (blue and red traces) and non-responsive (black trace) cells in **D**.

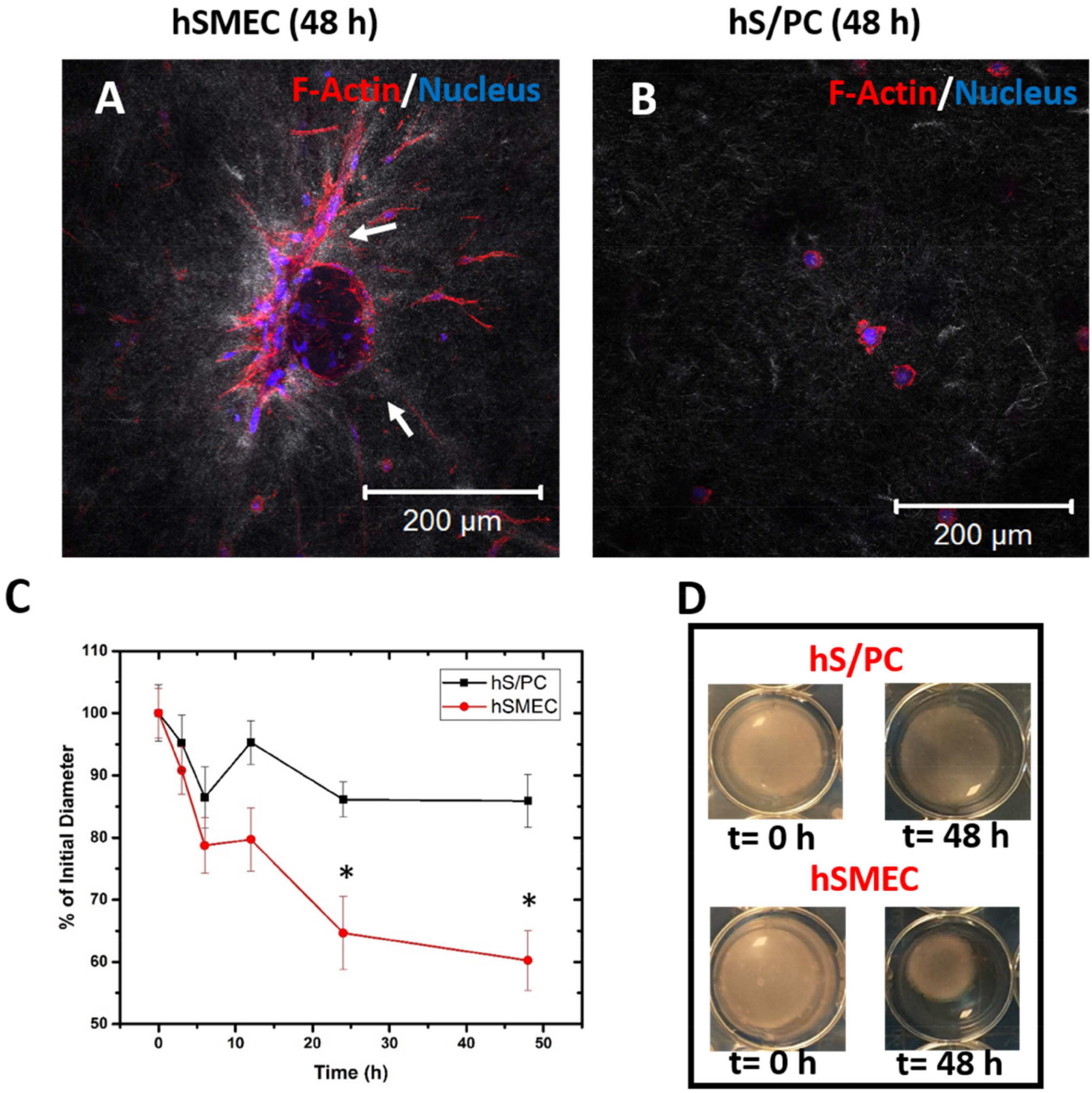


**Figure 3. Collagen gel contraction assay**

**(A-B)**. Differential reflectance confocal microscopy of hSMECs (A) and hS/PCs (B) cultured in collagen gels. F-actin and nuclei were stained red and blue, respectively, while collagen fibrils appeared grey (**C-D**). Reduction of the diameter of cell-laden collagen gels as a semi-quantitative assessment of hS/PCs and hSMECs contractility. The gross appearance of the gel constructs at 0 h and 48 h is shown in D. *: statistically significant when compared to hS/PC at the same time point, $p<0.05$

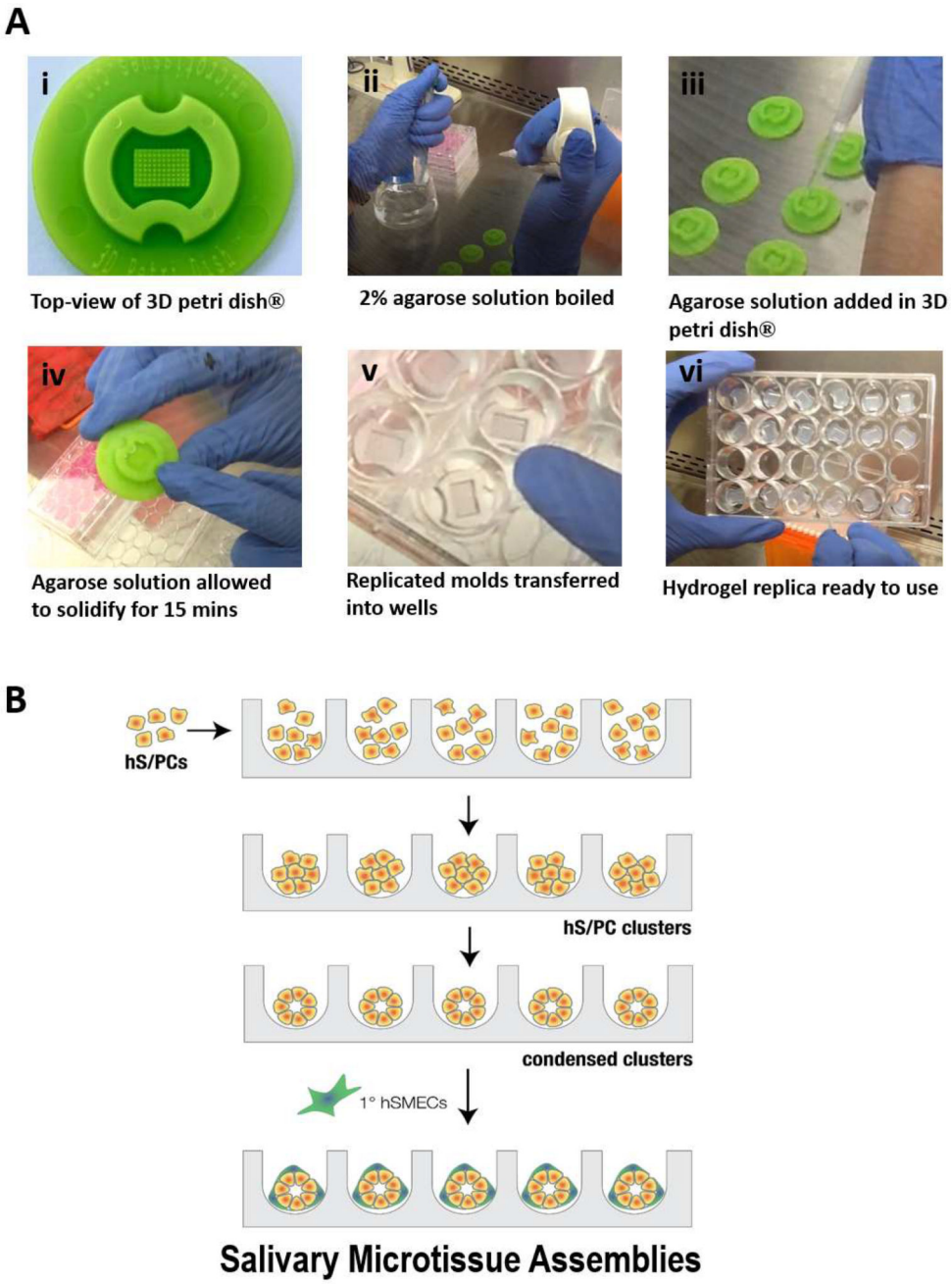


**Figure 4. Step-wise assembly of salivary gland microtissues using agarose-replicated microwells**

**(A)** Photographs showing the hydrogel replication protocol. A commercial 3D petri dish® (i) was used as the mold. Sterilized molds were placed in a laminar flow hood and 2% agarose was brought to a boil (ii). The agarose solution was then added into the mold (iii). After the solution solidified (iv), the hydrogel replica was removed from the mold and transferred to a 24-well plate (v-vi) for cell assembly. **(B)** Schematic depiction of the bottom-up assembly process. Homogenously dispersed hS/PCs were counted and seeded in the microwell at a predetermined cell concentration for the targeted spheroid diameter. After an initial incubation period, cells aggregated and compacted into tight spheroid structures.

Following spheroid formation, myoepithelial cells were added to the tight structures to form the microtissues.

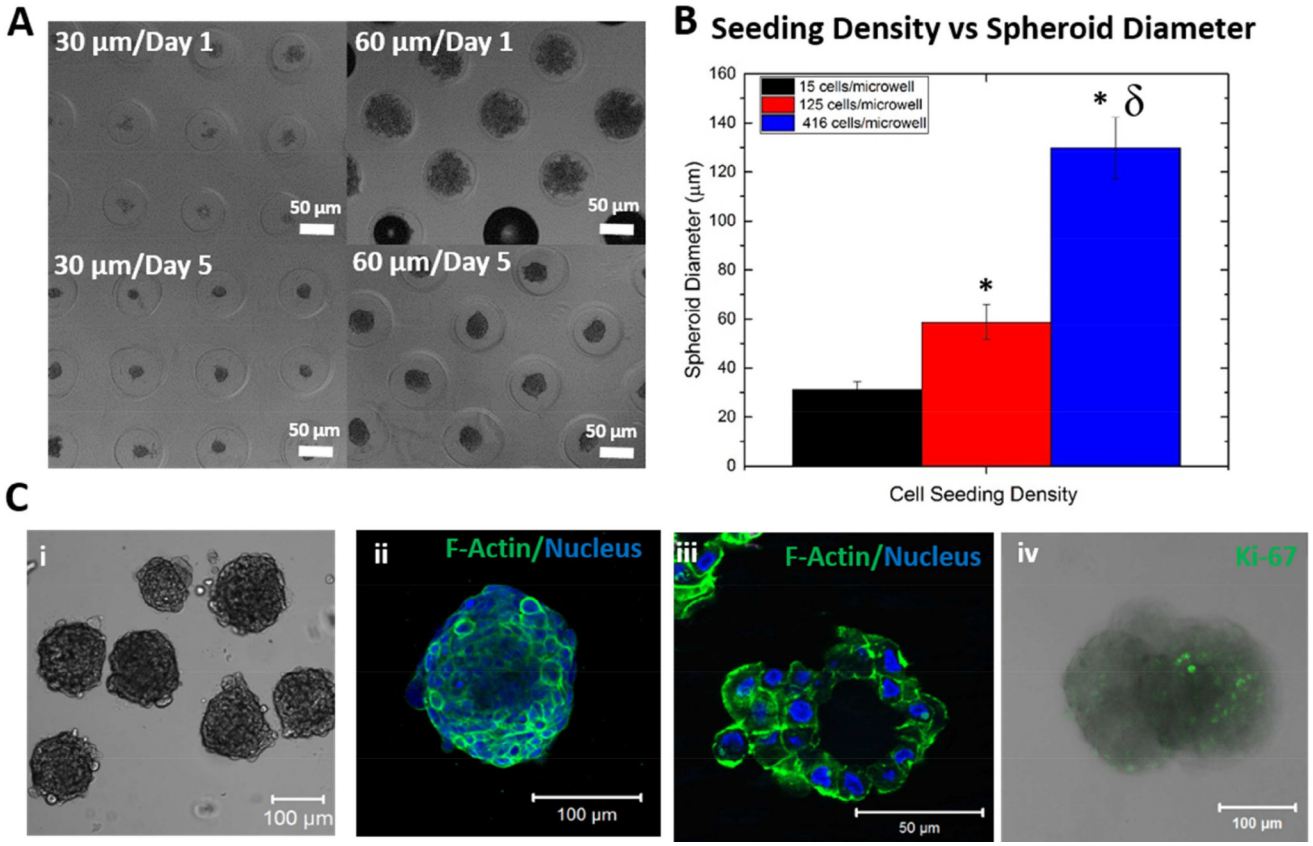


**Figure 5. Construction of hS/PC spheroids**

**(A-B)**. Spheroid diameter was adjusted by changing the initial cell seeding density (A), and the average spheroid diameter for a given cell seeding density was calculated (B, *:significantly different from spheroids with 30 µm diameter $p<0.05$, δ: significantly different from spheroids with 60 µm diameter $p<0.05$). **(C)** Microscopic observation of hS/PC spheroids. The bright field image shows the gross appearance of assembled structures. Confocal images were acquired on the entire spheroid as a Z-stack (ii) and on a cryosectioned slice to show the central lumen (iii). F-actin and nuclei were stained green and blue, respectively. The combined fluorescence and bright field image (iv) showed the presence of proliferative cells, stained green for Ki67.

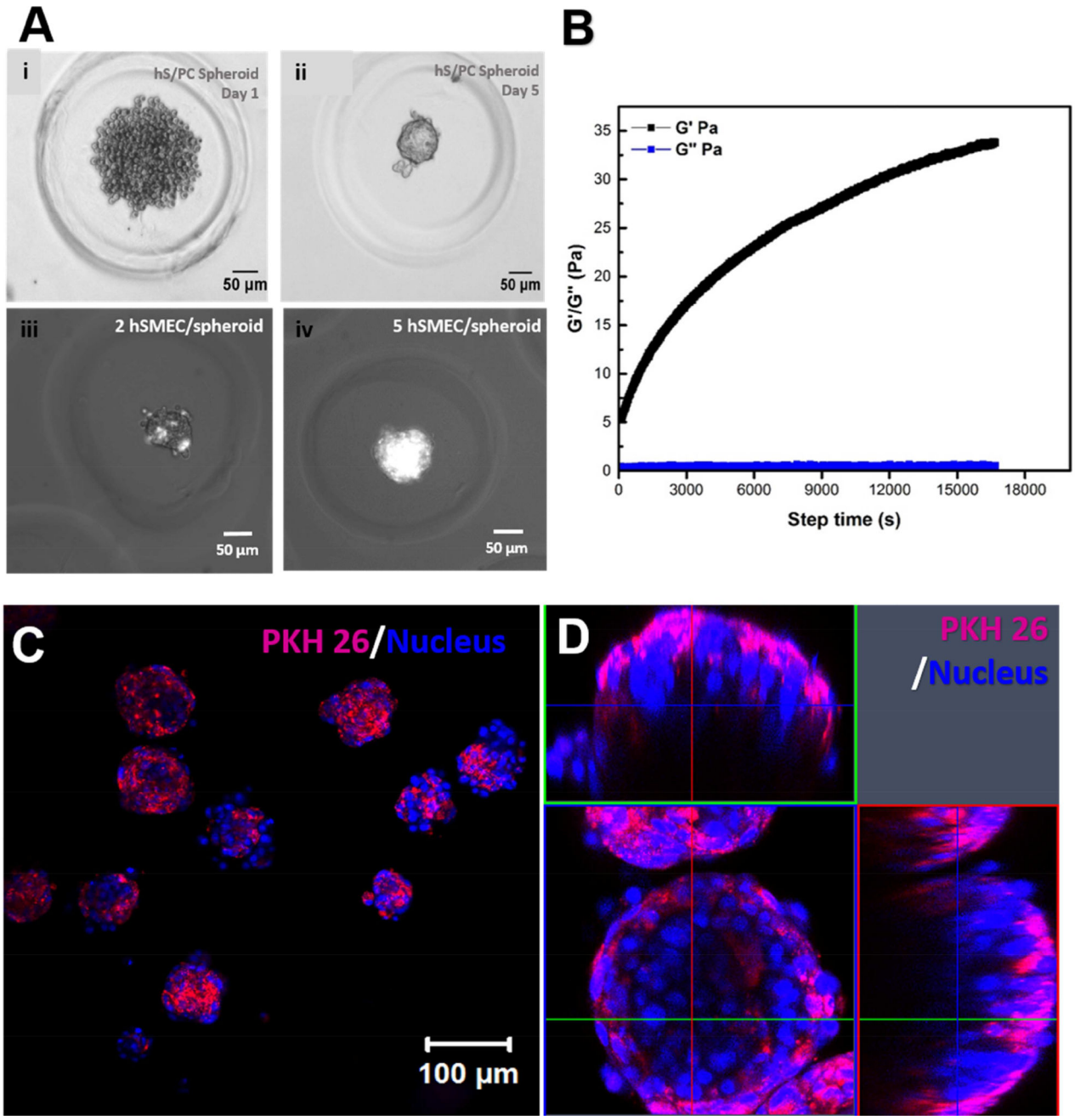


**Figure 6. Morphological characterization of hS/PC-hSMEC co-assemblies**

**(A)** Evolution of the microtissue from the initial loose hS/PC aggregates (i), to compact spheroids (ii), and the optimization of hSMEC/spheroid ratio to achieve a complete coverage of hS/PC spheroids by hSMECs (iii, iv). (B). Rheological characterization of HA/PEG gels used to encapsulate the assembled microtissues. A representative time-sweep result is shown. **(C, D)** Confocal images of 3D encapsulated salivary gland microtissues at low (C) and high magnifications (D). Expanded horizontal and vertical views shown in D revealed the spatial arrangement of the two cell types in the microtissue. hSMECs (labeled magenta with PKH26) localized on the outer surface of the structure. Cell nuclei were stained blue.

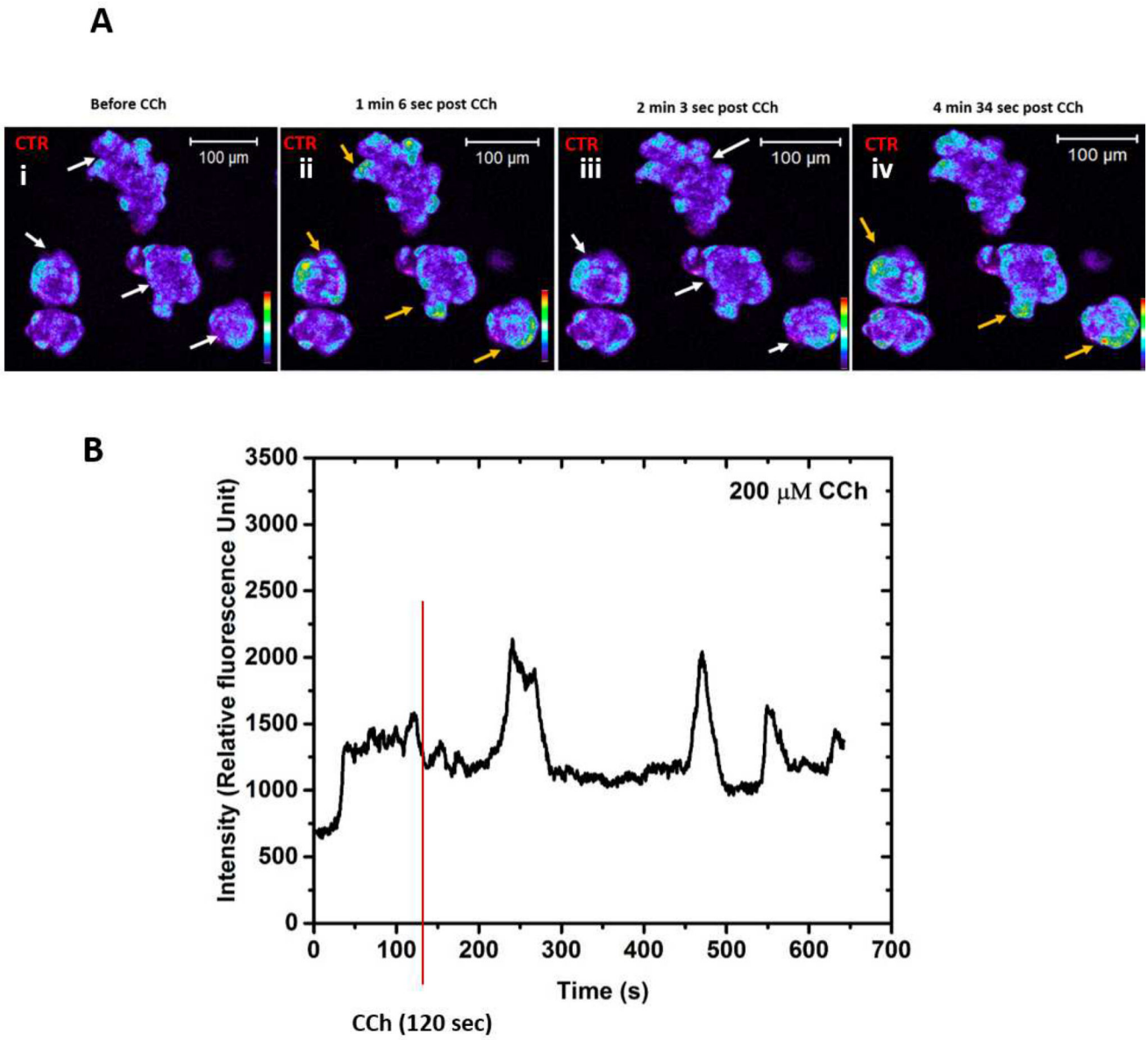


**Figure 7. Intracellular calcium imaging of the hS/PC-hSMEC co-assemblies**

**(A)** Confocal color scale spectrum of time dependent [$Ca^{2+}_i$] fluorescent intensities are shown in blue to deep orange and hSMECs in red (CTR). White arrows indicate decrease in the [$Ca^{2+}_i$] signals, orange colored arrows indicate increase in the [$Ca^{2+}_i$] signals. **(B)** The relative fluorescence intensity acquired from the live cell videos from microtissues as a function of time upon CCh treatment.

## Table 1

Primer sequences used in the qPCR experiments

| Genes | Forward primer (5'-3') | Reverse primer (5'-3') | Product size (bp) |
|---|---|---|---|
| GAPDH | CAGCCTCAAGATCATCAGCA | TGTGGTCATGAGTCCTTCCA | 106 |
| KRT5 | CGTGCCGCAGTTCTATATTCT | ACTTTGGGTTCTCGTGTCAG | 82 |
| KRT14 | CACAGATCCCACTGGAAGAT | GATAATGAAGCTGTATTGATTGCC | 101 |
| ACTA2 | GACTTCCGCTTCAATTCC | GTTAGGACCTTCCCTCAG | 177 |
| MYC11 | AGATGGTTCTGAGGAGGAAACG | AAAACTGTAGAAAGTTGCTTATTCACT | 85 |

Gene symbols: KRT5: Cytokeratin 5, KRT14: cytokeratin 14, ACTA2: alpha-smooth muscle actin, MYC11: myosin heavy chain 11.